

Aero-acoustic levitation: A method for containerless liquid-phase processing at high temperatures

Cite as: Review of Scientific Instruments **65**, 456 (1994); <https://doi.org/10.1063/1.1145157>
Submitted: 30 June 1993 . Accepted: 01 November 1993 . Published Online: 04 June 1998

J. K. Richard Weber, D. Scott Hampton, Dennis R. Merkley, Charles A. Rey, Mark M. Zatarski, and Paul C. Nordine



View Online



Export Citation

ARTICLES YOU MAY BE INTERESTED IN

[Compact acoustic levitation device for studies in fluid dynamics and material science in the laboratory and microgravity](#)

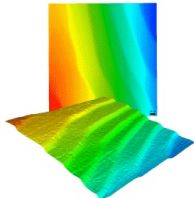
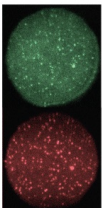
Review of Scientific Instruments **56**, 2059 (1985); <https://doi.org/10.1063/1.1138419>

[Parametric study of single-axis acoustic levitation](#)

Applied Physics Letters **79**, 881 (2001); <https://doi.org/10.1063/1.1391398>

[TinyLev: A multi-emitter single-axis acoustic levitator](#)

Review of Scientific Instruments **88**, 085105 (2017); <https://doi.org/10.1063/1.4989995>

	<p>Nanopositioning Systems</p> 	<p>Modular Motion Control</p> 	<p>AFM and NSOM Instruments</p> 	<p>Single Molecule Microscopes</p> 
---	--	---	---	--

Aero-acoustic levitation: A method for containerless liquid-phase processing at high temperatures

J. K. Richard Weber,^{a)} D. Scott Hampton, Dennis R. Merkley, Charles A. Rey, Mark M. Zatarski, and Paul C. Nordine^{a)}

Intersonics, Inc., 3453 Commercial Avenue, Northbrook, Illinois 60062

(Received 30 June 1993; accepted for publication 1 November 1993)

A method for containerless liquid-phase processing was developed which has practical application in process and property research on virtually any material which is involatile at the melting point. It combines aerodynamic and acoustic forces to support and position the levitated material. The design provides forced convection control of the thermal boundary in the gas surrounding beam-heated specimens, which stabilizes the acoustic forces and allows acoustic positioning necessary to stabilize the aerodynamic levitation forces on molten materials. Beam heating and melting at very high temperatures was achieved. Experiments were conducted on specimens with diameters in the range 0.25–0.4 cm, of density up to 9 g/cm³, at temperatures up to 2700 K, and in oxygen, air, or argon atmospheres. Unique liquid-phase processing results included deep undercooling of aluminum oxide, glass formation at exceptionally small cooling rates, complete melting and undercooling of YBa₂Cu₃O_x superconductor materials, direct formation of the YBa₂Cu₃O_x from the liquid phase, and the vaporization of volatile constituents from a low-liquefaction point glass to form a refractory, high melting material. The application of rapid containerless batch processing operations to materials synthesis is discussed.

I. INTRODUCTION

Containerless experimental methods^{1,2} provide access to unique environments in the study and processing of molten materials at high temperatures. They achieve freedom from contamination due to reaction with containers and allow bulk purification by vaporization or gasification processes. Undercooling of the liquid is facilitated, typically to about 80% of the melting temperature, so that properties and processes can be investigated under conditions far from equilibrium. Good mechanical and optical access can be obtained with freely levitated specimens, and novel experiments to measure material properties and develop new processing operations become possible. In combination, these qualities of containerless experiments create a whole new way of investigating and processing materials at high temperatures.

In practice, containerless experiments are constrained by the properties of the material of interest. Electromagnetic levitation and heating^{3–12} has been used with metallic substances to melt,⁴ purify,⁵ undercool liquids,⁶ make glasses⁷ and single crystals,⁸ and measure properties such as surface tension,⁹ mixing¹⁰ and fusion¹¹ enthalpies, liquid heat capacity,^{11,12} and optical properties of clean liquid metal surfaces.⁵ However, a versatile method for containerless experiments on molten dielectric materials has not been available.

Dielectric materials have been levitated by methods which employ acoustic,^{13–18} electrostatic,^{19–23} or aerodynamic forces^{24–29} to support and position specimen materials, which were heated and melted in either a furnace or by beam-heating methods. Acoustic levitation is possible

on solids but the acoustic intensities required to levitate higher density materials result in large surface oscillations leading to fragmentation of liquid drops. This problem did not develop in the low gravity environment of space where smaller acoustic intensities were used for levitation positioning of glass forming melts in a furnace at temperatures up to 1500 °C.³⁰ Gas jet levitation provides large forces capable of levitating beam-heated solids, but becomes unstable when the levitated material melts. Aerodynamic levitation of 2–5 mm diameter specimens in conical nozzles has been used with liquid aluminum and uranium which were electromagnetically heated,²⁴ and with laser beam-heated oxide materials.²⁸ Gas-film levitation²⁹ has been developed for application to larger masses of material that are heated, melted, and supported out of contact with a shaped porous container through which gas flows. Electrostatic levitation has been applied to position small particles of dielectric materials and study their transient behavior upon rapid heating with a laser beam,^{21,22} which resulted in levitation instabilities. More recently, stable, long-term electrostatic levitation and arc-lamp beam heating and melting of zirconium in a high vacuum system was reported.²³

This paper describes a new, hybrid method for containerless experiments, called aero-acoustic levitation (AAL), which can be used to levitate, heat, and melt any involatile material. The AAL method uses aerodynamic and acoustic forces in combination to make each work better than it would alone. A gas jet flow is used to produce aerodynamic forces to support the levitated specimens. When the specimens are beam heated, the gas flow results in a stable and thin thermal boundary layer and eliminates natural convection instabilities that would interfere with control of the acoustic forces. The specimen position, rotation, and shape are controlled by these acoustic forces so

^{a)} Present address: Containerless Research, Inc., 910 University Place, Evanston, IL 60201-3149.

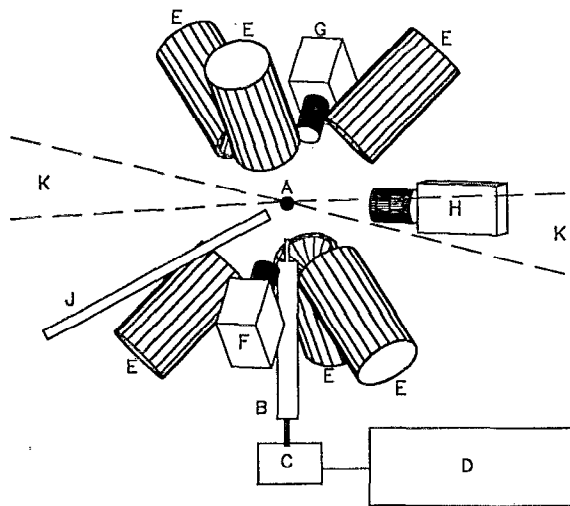


FIG. 1. Schematic of the aero-acoustic levitator. *A*, levitated specimen; *B*, gas flow tube and heater; *C*, translation stage; *D*, flow control system; *E*, acoustic transducers (three axis); *F*, diode laser specimen illuminator (3 axis); *G*, specimen position detector (3 axis); *H*, video camera; *J*, vacuum chuck; *K*, laser beam heating.

that the aerodynamic forces and levitation remain stable when the specimen melts.

The AAL device is described and its uses illustrated by experiments conducted on dielectric materials of sample diameters in the range 0.25–0.4 cm and density up to 9 g/cm³ that were cw CO₂ laser beam heated and melted at temperatures up to 2700 K and processed in oxygen, air, or argon atmospheres. The method provided excellent optical and mechanical access to the levitated specimens.

II. EXPERIMENTAL

A. Method

A schematic illustration of the aero-acoustic levitator is presented in Fig. 1. The device combined a three-axis, opposed-transducer, nonresonant acoustic positioner with an aerodynamic levitator comprised of a hot vertical gas jet. The acoustic positioner created an array of nodes in which specimens may be located and the gas jet levitator provided the lift force to support a specimen in the vicinity of one of the nodes. Position detection and control devices were used to stabilize levitation of the specimens. A cw CO₂ laser beam was split and focused onto opposite sides of the levitated specimen for heating and melting experiments. Video cameras with automatic irises were used to observe and record specimen motions in the horizontal plane and an automatic optical pyrometer measured and recorded the specimen temperature. A vacuum chuck mounted on a linear translator was used for specimen insertion and retrieval.

The acoustic positioner had three pairs of acoustic transducers on orthogonal axes perpendicular to the faces of a cube with a diagonal parallel to the vertical gas jet. The acoustic transducers created an array of higher- and lower-pressure regions, or nodes, capable of levitating solid and low-density liquid specimens. The gas jet levitator pro-

vided lift forces sufficient to support a dense specimen in the vicinity of one acoustic node. Specimen position was sensed by diode laser shadowing onto three position detectors on axes perpendicular to the three acoustic axes. The position detector signals were used to control the acoustic node positions to help keep the specimen position constant. Tangential forces on the specimen could be produced acoustically and were controlled to reduce specimen rotation prior to melting. The acoustic forces also reduced shape oscillations in levitated liquid drops. These capabilities allowed laser beam heating and melting of freely suspended materials and stable, long-term levitation of the molten drops. Levitation of laser beam-heated liquid drops was not stable with the acoustic or gas jet levitator operated alone.

The acoustic field was nonresonant, i.e., it was created by the direct output of the transducers and did not employ a tuned cavity in which a standing wave is created as in resonant acoustic levitators.^{14–16} The acoustic node positions were insensitive to the location of small objects within the field such as the vacuum chuck used for specimen insertion and retrieval.

The acoustic transducers were tuned to resonate at ~22 kHz, which is nominally above the audible frequency range. They were made from solid aluminum alloy, driven at the same frequency by piezoelectric transducers, shaped to match impedance with air at a thin, flared peripheral section, and cooled by forced convection. Back reflections of incoming sound waves were reduced by sound absorbing material placed in the central 4.4-cm-diam sections of the 7.0-cm-diam transducer surfaces. Node locations were controlled by adjusting the phase difference between opposed transducers on each acoustic axis and specimen rotation was controlled with the phase differences between sets of transducers on different axes.

Levitation occurred in a gas flow (jet) formed by a 0.229 ± 0.003 cm inside diameter by 20-cm-long mullite tube mounted vertically onto a three-axis translation stage. The tube was wrapped with a Nichrome wire heating element and thermal insulation to heat the levitation gas flow to temperatures up to 400 °C.

The nominal position at which specimens were levitated was 2.5 cm above the gas flow tube in the horizontal plane of the laser beams used for heating and melting. Alignment in this plane was achieved by translating the gas jet apparatus and adjusting the gas flow rate which was manually controlled during the experiments.

Maximum levitation stability occurred when the acoustic forces were controlled to locate the specimen at the same position that the gas jet would support it in the absence of acoustic positioning. The smallest position and velocity fluctuations in specimen position were then observed. The feedback control system for acoustic positioning was designed to achieve this position by adjusting the phase difference between opposed transducers in response to velocity of the specimen along each of the acoustic axes.

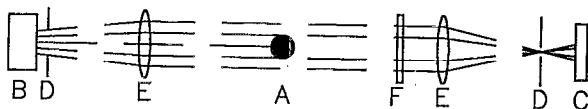


FIG. 2. Schematic of the position detector system. *A*, levitated specimen; *B*, diode laser specimen illuminator (3 axis); *C*, specimen position detector (3 axis); *D*, apertures; *E*, lens; *F*, spectral filter.

B. Specimen position detection and control

Preliminary experiments were conducted by using position sensitive detectors onto which the specimens were imaged using emitted or reflected light. This method worked well for materials which emitted or reflected light uniformly but materials which illuminated the detectors unevenly due to surface property variations could not be precisely positioned. Background radiation and the large dynamic range required with this method were further problems and position detection with reflected light did not work well at lower temperatures for glass materials or on oscillating liquid drops.

The method of laser shadow imaging was developed to obtain position detection independent of the levitated object's surface properties. The design is illustrated in Fig. 2. Modulated laser beams were used with spectral, spatial, and electronic filtering to discriminate against light emitted by the levitated specimen. The diode lasers operated at a wavelength of 780 nm and the beams were apodized to produce ~1 mW power and nearly uniform intensity over a 1 cm square region that surrounded the specimen. Spectral filtering was accomplished with a 700 nm infrared cut-on filter and the ~1060 nm limit for the silicon detectors. A lens imaged the specimen onto the position sensitive detectors through an aperture (spatial filter) which passed the laser light collected by the lens while rejecting most of the incandescent radiation.

The spatial filter discriminated against laser light scattered by refractive index variations in the vicinity of hot specimens. Increased noise in the positioning signals and decreased specimen stability was observed when the spatial filter was removed.

Negative feedback control of the acoustic node positions was applied in response to the time derivative of specimen position. This placed the average acoustic node position on the jet axis where radial velocity fluctuations were symmetrical.

The feedback control system was sensitive to the higher velocities produced by small, higher-frequency position fluctuations and insensitive to the lower velocity axial position changes induced by heating and melting. This limited the rate at which the acoustic node position changed in the axial direction in response to changes in the aerodynamic levitation force as the specimens were heated and melted. Manual control of the gas flows were sufficient to maintain the specimen at a fixed axial position.

C. Gas flow control

The gas flow rate was proportional to and measured by the pressure upstream of a metering orifice operated in

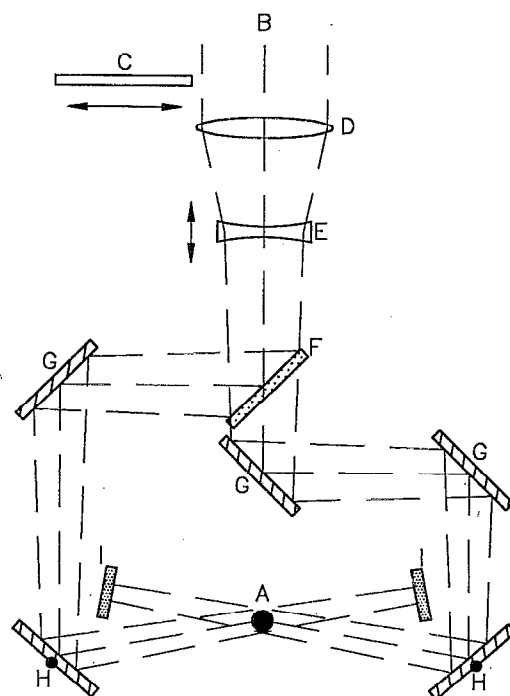


FIG. 3. Schematic of laser beam-heating system. *A*, levitated specimen; *B*, cw CO₂ laser beam; *C*, laser beam shutter; *D*, ZnSe lens of 50 cm focal length; *E*, ZnSe lens of -20 cm focal length; *F*, laser beam splitter; *G*, mirrors; *H*, gimbaled mirrors; *I*, beam stops.

critical flow. This pressure was controlled manually by a needle valve between the metering orifice and an air, oxygen, argon, or helium supply at ~4 bar pressure.

At a constant gas flow rate, the aerodynamic lift force decreased with the specimen temperature and increased with the shape changes that occurred when a specimen was first melted. These changes in the levitation force produced slow changes in the levitation height which were compensated for by changing the gas flow rate. Resolidification of the melt produced a solid of the same shape. Changes in the gas flow rate were not necessary when the specimen was quickly melted again.

D. Beam heating

Preliminary experiments were conducted with three arc lamps and three reflectors for six-sided beam heating of the levitated specimens. This method was applied in combination with specimen position detection and control via light emitted or reflected from the specimens. Levitation and melting of materials was achieved with this approach. However, the maximum temperature was limited to ~2000 °C, the reflected light interfered with temperature measurements by optical pyrometry, and the heating apparatus interfered with optical and mechanical access to the specimens. Therefore, the method of cw CO₂ laser heating described below was developed.

Figure 3 illustrates the cw CO₂ laser heating apparatus. The heating laser beam was provided by a Photon Sources Model 300 laser located in the adjoining room. The incoming beam passed through a telescope with ZnSe

lenses and was then split into two beams that were steered onto opposite sides of the specimen. The incident beams were separated by an angle of $\sim 170^\circ$ in the horizontal plane. Beam stops were provided to collect the laser energy that passed the levitated specimen. Operator controls were provided to vary the incident laser power from ~ 80 to 270 W, to continuously change the incident beam size with a motor-driven lens translator, and to operate a laser beam shutter. The intensity ratio for the two incident beams was ~ 1.5 . Some experiments used a retroreflector in place of one of the beam stops to increase the uniformity of heating. The retroreflector also increased the maximum temperature that could be achieved.

E. Instrumentation

Video images of the specimen were acquired by two CCD cameras sighting orthogonal views of the levitated specimen in the horizontal plane, on axes that were at $\sim 45^\circ$ to the heating laser beam axes. The video cameras had automatic irises, automatic electronic gain control (AGC), and gamma-response circuitry (for selection of linear or nonlinear, compressed response), which provided the high dynamic range needed for imaging over the large range of light intensity emitted by the specimens. A video recorder, multiplexer, and printer were provided to continuously record images of the specimen and to print selected images.

An optical pyrometer was developed for recording temperatures at high rates. It used a silicon detector, operated at a wavelength of 650 nm, and measured the temperature of a 1 -mm-diam spot on the levitated specimens. The lowest temperature range was ~ 1000 – 1900 °C. Neutral density filters extended the measurement range to higher temperatures. The pyrometer was calibrated against a NIST-traceable disappearing filament pyrometer using a tungsten strip lamp.

A laboratory computer was provided to acquire temperature data. It allowed temperature measurements at rates up to 1 kHz, for use in rapid cooling and heating experiments. The computer was interfaced to insert date, time, temperature, experimental identification, and other information on the video record which were updated at a frequency of 1 Hz.

F. Procedures

The materials processing experiments were conducted using air, oxygen, or argon as the levitation gas. The procedures were as follows.

The acoustic positioner was set to provide forces sufficient to acoustically levitate materials of density ~ 1 g/cm³. An approximately spherical specimen was inserted into the gas jet with the vacuum chuck and levitated. The acoustic intensity was adjusted and the feedback parameters on the position sensing control system were set to provide sufficient restoring force and control to stabilize the levitated specimen. Fine adjustments to the gas flow were then made to center the specimen image at the correct location on the video display and position it at the correct

position for laser heating. This procedure reproducibly located the specimen within about ± 0.05 of its radius from the design position, which was maintained during heating and melting by further changes in the gas flow rate.

Specimen rotation was reduced by manually adjusting the phase differences between the three sets of opposed acoustic transducers. This was more easily accomplished for imperfect spheres than for spheres. If the specimens were spheres, it was necessary to first heat them carefully to obtain a small shape change due to partial melting and resolidification, so that rotation could be controlled.

After rotation was sufficiently reduced, the specimens were rapidly melted by increasing the laser power or intensity. Liquefaction was easily accomplished with aluminum oxide which melts congruently. Experience was necessary to determine the correct laser intensity changes for incongruently melting materials like the ceramic superconductor which exhibited an ~ 250 °C melting range.

Rotation about horizontal axes ceased when slowly rotating specimens were melted, and an internal circulation of fluid developed as a result of the levitation gas flow over the liquid surface. The fluid circulation, and rotation of the liquid drop about the vertical axis, could be suppressed or enhanced by adjusting the phase differences between the acoustic transducers.

Superheating, undercooling, and other processing operations were conducted on the molten drops. Video records of the experiments were obtained, which included specimen position and motions, commentary, the date, time, and experimental identifier. Temperature measurements were also recorded on the video tape for most of the experiments. The acoustic positioning control parameters, laser power, flow rates, and levitation height above the flow tube were also recorded.

Separate experiments were conducted to investigate levitation and positioning phenomena. Levitation height was measured versus the levitation gas temperature, specimen temperature, gas flow rate, and for different materials and gases. Levitation gas flow rates were also measured versus the acoustic intensity for different specimen temperatures. The acoustic forces were characterized by measuring the minimum acoustic intensity required to levitate different density materials, and by measuring the average acoustic intensity provided by single transducers with a calibrated Brüel and Kjær Type 4138 condenser microphone. The temperature of the gas jet was measured with a thermocouple versus distance from the flow tube, to determine rates of jet mixing with the ambient air.

G. Materials and processing experiments

Results in which five different materials were processed at high temperatures will be presented to illustrate the performance of the apparatus under a range of processing conditions. The materials processed at high temperatures and the experiments performed on them are described below. Melting points and densities of the materials, and specimen diameters are given in Table I.

Aluminum oxide. Spherical aluminum oxide specimens of 0.318 cm diameter were levitated, laser beam heated and

TABLE I. Properties of processed materials.

Specimen material	Melting point (K)	Density (g/cm ³)	Diameters (cm)
Aluminum oxide	2327	4.0	0.3, 0.4
Ceramic superconductor	1270–1520	5.5	0.25, 0.3
Calcium-gallia-silica	~1820	4.5	0.30–0.35
"Black glass"	~1200	2.6	0.3
Inconel	~1600	8.9	0.3

melted, and the liquid was superheated to temperatures up to 2700 K. Rapid temperature versus time measurements were obtained when the liquid was cooled by blocking the laser beam. The increase in temperature (recalescence) which occurred upon spontaneous crystallization of the undercooled melt was recorded. The solid specimens formed from the liquid had the same shape as the liquid drops.

Ceramic superconductors. Approximately spherical samples of the YBa₂Cu₃O_{7-x} superconductor material composition were first annealed at 1000 °C and then were rapidly heated and melted at temperatures up to 1800 °C. The melts were cooled by blocking the laser beam to observe undercooling and recalescence.

Calcium-gallia-silica glass. Oxide mixtures of composition 41.2CaO · 52.5Ga₂O₃ · 6.3SiO₂, mol % plus 0, 0.001, or 0.005 wt % platinum were heated, melted, and held at a temperature ~1900 °C for several minutes. The melts were cooled under containerless conditions by slowly decreasing the heating laser beam intensity. The recovered materials were visually examined for evidence of crystallization.

"Black glass." Glass samples of composition 69.7SiO₂, 15.2Na₂O, 3.4CaO, 1.3B₂O₃, 3.2BaO, 6.4MnO₂, 0.8K₂O, wt % was levitated, melted, and heated slowly to about 2300 K, 1100 °C above the liquefaction temperature. Evaporation of volatile components led to a large mass loss and decrease in the specimen size which required changes in the gas flow to maintain levitation.

Inconel. Inconel was heated and partially melted using an argon gas jet to levitate the specimen. Mixing of ambient air into the argon jet resulted in rapid oxidation of the specimen at the melting point and the experiment was terminated before melting was complete.

III. RESULTS

This section presents new results that were obtained to characterize levitator performance illustrate its use for liquid-phase processing. Detailed results of several liquid-phase processing investigations on aluminum oxide,³¹ calcium-gallia glass formation,³² and YBa₂Cu₃O_x materials^{33,34} are presented elsewhere.

A. Levitation

Acoustic positioning. Arrays of polystyrene specimens (typical density of 0.1 g/cm³) and water drops were levitated in the acoustic nodes produced by the three-axis levitator. The distance between levitated specimens was ~0.79 cm, half the acoustic wavelength in air. The entire

array could be translated within the region intercepted by the sound fields of the 7-cm-diam transducers, by changing the phase differences between opposed transducer pairs. Rotation of acoustically levitated specimens was also obtained, by controlling the phase differences between sets of opposed transducers. This rotation was observed by motion of the surface features on irregular solid objects. Centrifugal shape distortions occurred for rotating liquid drops. In separate experiments, vertical positioning was demonstrated over a distance of ~15 cm between a single pair of opposed transducers. Levitation was not possible within the near field (~3 cm) of the transducer surfaces. Levitation and positioning along a horizontal line was also possible for low-density polystyrene specimens with two horizontally mounted transducers.

Figure 4 presents calibration data for the acoustic positioning system. It presents (i) the average acoustic intensity from single transducers measured in the center of the acoustic field, and (ii) the maximum density of materials that could be levitated as a function of the control parameter on the acoustic driver which determined the intensity level. The levitation data were obtained on specimens of density from 1.0 g/cm³ (water) to 3.8 g/cm³ (96% dense aluminum oxide). Specimen diameters were ~0.30 cm.

Acoustically levitated water drops developed severe oscillations leading to loss of material when the acoustic intensity was increased to the levels required to levitate high-density solids. This occurred at sound pressure levels

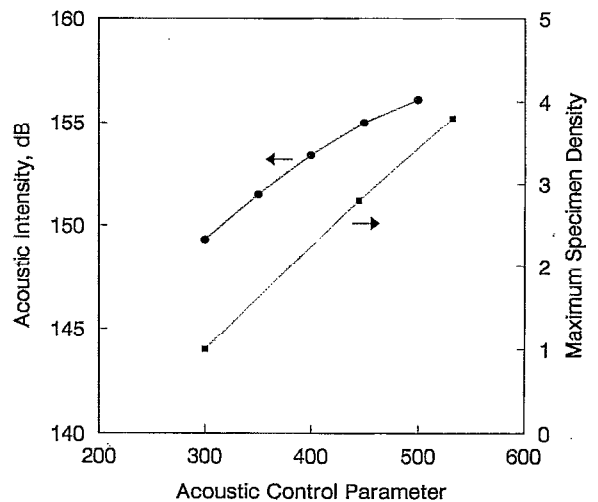


FIG. 4. Maximum specimen density and acoustic intensity vs the acoustic intensity control parameter.

TABLE II. Aerodynamic levitation in air.

Material and gas	Specimen		Gas		Specimen		<i>F</i>
	Diam. (cm)	Mass (g)	Flow rate (g/s)	Temp. (K)	Height (cm)	Temp. (K)	
Al ₂ O ₃ , air	0.318	0.0636	0.0600	520	1	300	2.87
	0.318	0.0636	0.0600	520	5	520	2.07
	0.318	0.0636	0.0581	520	1.1	520	1.94
Al ₂ O ₃ , He	0.318	0.0636	0.0252	480	1.3	480	2.44
	0.318	0.0636	0.0269	480	2.4	480	2.79
Al, air	0.318	0.0447	0.0504	520	2.9	520	2.07
	0.318	0.0447	0.0483	520	0.4	520	1.90
	0.318	0.0447	0.0536	520	4	520	2.34
Monel, air	0.318	0.141	0.0970	520	3.8	520	2.44

sufficient to levitate ~ 2.5 and ~ 4.5 g/cm³ specimens for 0.32- and 0.15-cm-diam drops, respectively.

Acoustic levitation became unstable when solid or liquid specimens were laser beam heated. This instability was attributed to unstable natural convection in the air surrounding the specimen which caused variations in the sound speed and acoustic node positions.

Aerodynamic levitation. Aerodynamic levitation of 0.318-cm-diam solid aluminum and aluminum oxide specimens was readily achieved using gas flow rates determined by experience and a levitation gas temperature of ~ 250 °C. The distance between the specimen and gas flow tube increased as the specimen was heated by the hot gas. A monel sphere of 0.318 cm was levitated for ~ 5 s. Its initial ± 1 cm axial position fluctuations increased as the specimen was heated by the hot gas flow and levitation failed after 5 s.

Table II presents conditions for aerodynamic levitation of several specimens in air and helium. The last column in the table gives the quotient of momentum flow rate in the jet and the specimen weight. This quantity was calculated from the equation

$$F = \frac{\dot{m}_j u_j}{Mg}, \quad (1)$$

where \dot{m}_j is the gas mass flow rate, u_j is the jet velocity at the flow tube exit, and Mg is the specimen weight.

Aero-acoustic levitation. Aero-acoustic levitation resulted in high stability for levitated specimens in argon or in air. The required acoustic intensity (acoustic control parameter = 325) was slightly greater than the minimum value for acoustic levitation of water drops at ambient temperature. Position fluctuations of ± 0.01 cm occurred at a frequency ~ 30 Hz in both radial and axial directions. Slower axial position variations as large as half the specimen diameter (~ 0.15 cm) also occurred as a result of changing levitation forces that were controlled by operator adjustment of the gas flow rate. Axial position control to ± 0.05 of the specimen radius was achieved for liquid specimens levitated at constant temperature.

Aero-acoustic levitation in helium was not successful even though aerodynamic levitation of aluminum oxide specimens was readily achieved. Large and rapid fluctua-

tions in the acoustic node position were produced when the specimen position detection and control system was turned on.

Figure 5 plots levitation height versus the quotient F of momentum flow rate in the gas jet and specimen weight, for a 0.318-cm-diam aluminum sphere with gas jet temperatures of 80 and 180 °C. Each curve shows transitional behavior between conditions where the levitation height displayed a strong and weak dependence on F . Similar results were obtained for a 0.318-cm-diam monel specimen using a gas temperature of 330 °C.

Figure 6 illustrates the variation of jet temperature with height above the flow tube for flow conditions near the knee in the curves of Fig. 5. Transitional behavior is also observed in these functions, with nearly constant jet temperature at smaller heights, and decreasing temperature at greater heights. The arrows mark the maximum height at which levitation was achieved in these gas jets.

The transitions between different functional dependencies of the levitation flow rate or gas temperature on height were attributed to a change from laminar to turbulent jet flow. The onset of turbulent jet flow resulted in more rapid

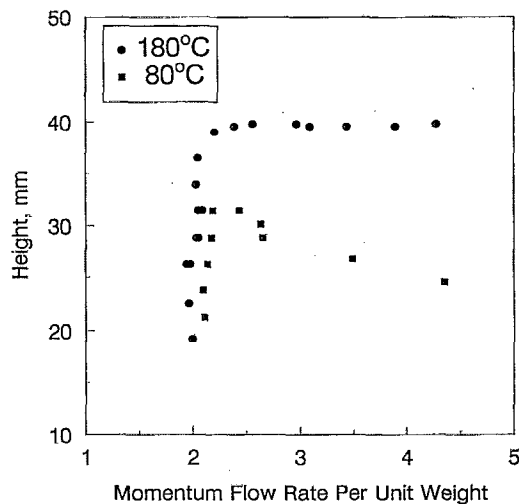


FIG. 5. Height above the gas flow tube vs the ratio of the gas momentum flow rate and the specimen weight for 0.318-cm-diam, 45 mg aluminum spheres in air.

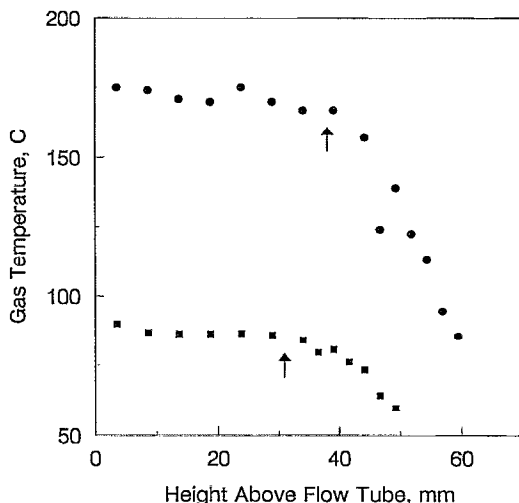


FIG. 6. Jet gas temperature vs height above the flow tube at air flow rates near the knee of curves in Fig. 5. Circles: $Re_d=1710$. Squares: $Re_d=1460$. The arrows mark the maximum levitation height.

mixing of the hot jet and cooler ambient gas to produce a more rapid temperature decrease and jet diameter increase with height and less efficient conversion of jet momentum into force on the levitated specimen.

In air, the transition between laminar and turbulent jet flow occurred at a height: nozzle diameter ratio (h/d) which increased as the jet Reynolds number (Re_d) decreased. The value of the product, $Re_d h/d$, was $\sim 24\,000$ near the knee in the curves of levitation height versus gas flow rate or gas temperature versus height. In helium, a smaller value, $Re_d h/d = 10\,500$, was obtained at the transition from laminar to turbulent jet flow found in the jet temperature versus height measurements.

Figure 7 presents aero-acoustic levitation results for laser beam-heated solid and liquid aluminum oxide specimens. The data for the liquid were obtained on a smaller

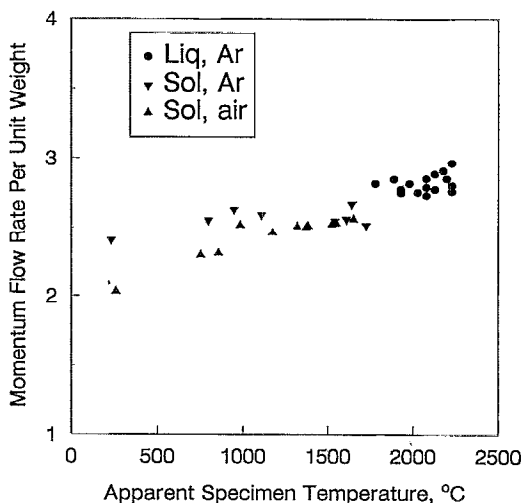


FIG. 7. Momentum flow rate vs specimen temperature for aluminum oxide specimens levitated in air or argon. Specimen mass: solid, 64 mg; liquid, 48 mg.

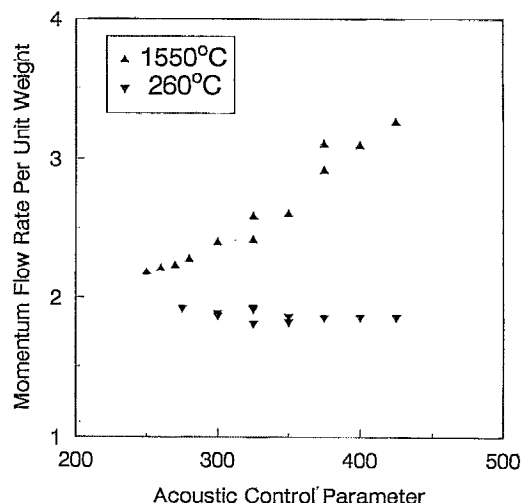


FIG. 8. Momentum flow rate vs acoustic intensity control parameter for aero-acoustic levitation of a 64 mg aluminum oxide specimen at the jet temperature (260 °C) and laser heated to 1550 °C.

specimen that those for the solid and show a slight increase in the value of F at the melting point. In fact, when a solid specimen sphere was melted without mass loss, an $\sim 10\%$ decrease in F was observed. These results showed that the levitation efficiency decreased slightly with temperature and increased with specimen size.

Figure 8 illustrates effects of the acoustic field on the aero-acoustic levitation efficiency in air. These results show that the levitation efficiency is nearly independent of acoustic intensity at low temperatures but decreases with the acoustic intensity for the laser-heated specimen at 1550 °C.

The results in Figs. 7 and 8 suggest that the acoustic field interacts with the specimen and gas flow in a manner that reduces the levitation efficiency. This conclusion is further supported by previous aerodynamic levitation results²⁵ which showed that the levitation efficiencies increase slightly with the temperature of laser heated specimens, in agreement with the result obtained by extrapolation of the data in Fig. 8 to zero-acoustic intensity. The smaller aero-acoustic levitation efficiencies in argon than in air also agree with the previous results²⁵ in ambient temperature subsonic gas jets at reduced pressures.

B. Energy balance

A molten 64 mg aluminum oxide specimen was maintained at a temperature near the melting point, in argon, with an incident laser power of 83 ± 5 W. A laser power increase to ~ 270 W was required to heat the liquid to its maximum temperature, 2700 K. The levitated drops cooled at rates up to 600 K/s when the laser beam was blocked. Cooling curves for aluminum oxide are presented elsewhere.³¹

C. Liquid-phase processing

Stable operation with molten black glass and partially molten aluminum oxide was possible with arc-lamp heating and position detection using light emitted and reflected

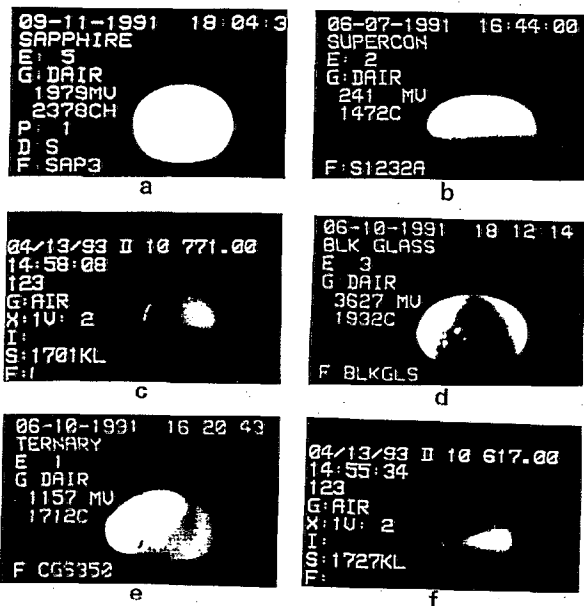


FIG. 9. Video images of levitated liquid drops. The largest diameter of the specimen in Fig. 10(b) is 0.440 cm and the scale is the same for all specimens. (a) 64 mg aluminum oxide at 2680 K, (b) 100 mg $\text{YBa}_2\text{Cu}_3\text{O}_x$ specimen at 1750 K, (c) 38 mg $\text{YBa}_2\text{Cu}_3\text{O}_x$ specimen at 1700 K, (d) bubble bursting at the surface of a 42 mg glass specimen at ~ 2200 K, (e) vortex formed in 110 mg calcia-gallia-silica melt at ~ 2000 K, (f) 38 mg $\text{YBa}_2\text{Cu}_3\text{O}_x$ specimen at ~ 1730 K. In (f), internal circulation was acoustically suppressed and the specimen was rotated about the vertical axis.

by the specimens. The substitution of cw CO_2 laser heating allowed complete melting of aluminum oxide. Laser shadowing for position detection allowed operation with transparent glass materials at lower temperatures, clear sapphire spheres, and ceramic superconductor materials which melted incongruently and exhibited large emissivity difference between the solid and liquid areas of the specimen. The liquid-phase processing experiments described in this section were conducted with the laser beam heating and laser shadowing position detection systems.

Video images of several liquid specimens during containerless processing are given in Fig. 9 and discussed in the following description of liquid-phase processing results. The images in Fig. 9 include numerical data inserted onto the video record, such as the specimen temperature, real time, and experimental identification numbers.

Melting. It was necessary to reduce the rotation rate of the levitated specimens prior to liquefaction, to avoid centrifugal ejection of small liquid drops. Congruently melting aluminum oxide spheres were easily liquified by increasing the laser power and making small changes in the gas flow rate as the liquid formed. Rapid melting of the hot levitated aluminum oxide in about one second was possible by making a sudden increase in the laser intensity. Incongruent melting of $\text{YBa}_2\text{Cu}_3\text{O}_x$ material occurred over a 200–250 °C temperature range as the temperature was increased at 50–100 °C/s. Liquefaction of the black glass material was a continuous process which occurred as the specimen was heated to form a viscous liquid drop.

The levitated liquid specimens had a shape determined

largely by surface tension and gravitational forces. Their shapes were similar to sessile drops with smaller specimens more nearly spherical than larger ones. The drop shapes for different materials illustrated in Fig. 9 indicate that the surface tension to density ratio for the liquids decreases in the order aluminum oxide > calcia-gallia-silica > $\text{YBa}_2\text{Cu}_3\text{O}_{7-\delta}$.

Vaporization. The black glass material began to vaporize at temperatures below the 1000 °C limit of the optical pyrometer. Bubbles formed as the specimens were heated to temperatures up to 2000 °C. The bubbles migrated slowly to and burst at the surface. The levitation gas flow rate was reduced as the specimen mass decreased by vaporization. A 20% decrease in diameter and $\sim 50\%$ mass loss occurred in one experiment, resulting in a high liquefaction temperature glassy material. Figure 9(d) was obtained just as a bubble burst at the surface of a levitated liquid drop of the black glass material.

Small vaporization mass losses occurred for aluminum oxide and calcia-gallia-silica melts held at high temperatures for several minutes. The $\text{YBa}_2\text{Cu}_3\text{O}_x$ materials exhibited larger mass loss rates, but showed no change in relative Y-Ba-Cu content if melting and resolidification were accomplished in less than one minute.

Undercooling. Molten aluminum oxide remained liquid to temperatures ~ 400 °C below the melting point when cooled under containerless conditions. Liquid $\text{YBa}_2\text{Cu}_3\text{O}_x$ compositions were also undercooled such that spontaneous crystallization of the undercooled melt led to direct formation of tetragonal $\text{YBa}_2\text{Cu}_3\text{O}_x$ crystals. Sufficient undercooling of these materials led to spontaneous crystallization and a temperature increase (recalescence) to the liquidus temperature.

Glass formation. The material remaining after vaporization of volatile components from the black glass material had a glassy, off-white appearance. It was evidently composed of the less volatile components of the black glass, mainly SiO_2 .

Glass was formed from the molten calcia-gallia-silica mixtures at the lowest cooling rates investigated. With 1 ppm Pt additions to the melt, glass formed at cooling rates of less than 10 °C/s. Addition of 5 ppm Pt resulted in glass formation at cooling rates of 40–80 °C/s. The minimum cooling rate for glass formation from these materials as pendant drops attached to Pt-Rh thermocouples are greater than 300 °C/s.³⁵

Stirring. The gas flow over the levitated liquid drops produced an internal circulation like that which occurs in a falling liquid drop. When the heating laser beams were focused onto small spots at the specimen surface, a vortex could often be observed where the hot fluid arising from the laser heated regions mixed with the cooler bulk liquid. Such a vortex is illustrated in Fig. 9(e) which shows a molten calcia-gallia-silica specimen at a bulk temperature ~ 1700 °C.

Figure 9(f) illustrates a liquid $\text{YBa}_2\text{Cu}_3\text{O}_x$ drop in which the internal circulation was reduced and rotation about the vertical axis was induced by the acoustic forces. The larger temperature gradients which occurred in un-

stirred drops are evident by the colder (darker appearing) regions at the bottom and top portions of the specimen. Enhanced stirring resulted in more uniform specimen temperatures.

Shaping. Approximately equal acoustic intensities led to drop shapes that were symmetrical about the vertical axis and independent of the acoustic intensity. The use of unequal intensities between the three orthogonal acoustic axes provided some control of the drop shape. Flattened and elongated levitated liquid drops could be formed. Drop shaping effects were small at the acoustic intensities normally used in aero-acoustic levitation (sufficient to acoustically levitate liquid water drops), and increased with the acoustic intensity.

Liquid breakup. Oscillations in liquid drops and levitation instability occurred when the acoustic intensity was increased above a limiting value that depended on the levitated material, the liquid drop size, and the temperature. Breakup of the liquid drops occurred as the acoustic intensity was increased above this limit. A smaller levitated drop usually resulted, which was stable and did not oscillate until the acoustic intensity was increased again.

Rapid melt processing. The decrease in the required levitation gas flow that occurred upon melting of an aluminum oxide specimen was approximately equal to the increase in gas flow with temperature required to maintain the levitation height when the levitated solid was slowly heated to the melting point. Since the axial position changed only slowly with time, rapid heating and melting, or solidification of a liquid drop and cooling was possible without any adjustments to the gas flow rate. Rapid processing was accomplished by opening the laser beam shutter for a few seconds. In this way, aluminum oxide specimens were heated, melted, superheated to ~ 2700 K, undercooled to ~ 2000 K, solidified, and the solid cooled to temperatures below 1000 K within 6 s.

IV. DISCUSSION

Aero-acoustic levitation and melting of beam-heated specimens was easily accomplished in this work. The method worked the first time it was tried, on a glass material which formed a viscous liquid, using arc-lamp heating and specimen position detection via light emitted from the sample. A key early innovation was the use of a heated gas jet, which reduced the jet Reynolds number and maintained laminar flow of the levitating gas stream. This allowed higher density materials to be levitated by simply heating the gas to increase its viscosity and decrease the jet Reynolds number. Later addition of cw CO₂ laser heating and laser shadowing for position detection extended operation to lower viscosity melts and materials of nonuniform emissivity.

Apart from the need for appropriate controls in the acoustic stabilizing system, there are three key design criteria for aero-acoustic levitation. First, the acoustic intensities should be sufficient to acoustically levitate materials of density 1–2 g/cm³. This will occur if the acoustic intensities up to 150 dB can be obtained at the levitation position from each acoustic transducer. Second, the momen-

tum flow rate in the aerodynamic levitation jet should be about twice the specimen weight. This applied for the present case with values in the range 1.3–1.7 for the specimen: jet nozzle diameter ratio. Greater values of the quotient of momentum flow rate and specimen weight would be required for smaller specimen: nozzle diameter ratios. Third, the product of levitation height and Reynolds number for the gas jet should not exceed a certain value which was $Re_d h/d \approx 24\,000$ for levitation with air.

The use of aerodynamic and acoustic forces in combination succeeded under conditions where neither method would work by itself. Each made the other stable. The upward flowing gas provided sufficient lift to overcome most of the weight of the specimen. Small acoustic forces were then sufficient to stabilize the specimen position, supplement the surface tension of liquids to control specimen shape, and thus achieve stable levitation of melts. Simultaneously, the forced convection gas flow produced a stable thermal boundary layer in the gas around the specimen, and a stable (but nonuniform) sound speed in the vicinity of the levitated specimen, resulting in precise control of the acoustic forces.

Sound speed differences between the levitation gas flow and ambient air may have been the primary source of differences in the aero-acoustic levitation behavior in air, argon, and helium. These differences resulted from both temperature and atomic or molecular weight differences between the gases. They were greatest in helium, for which aero-acoustic levitation was not possible even though aerodynamic levitation was readily achieved. Figure 7 shows that the specimen temperature dependence of levitation efficiency was smaller in argon than in air, which may be due to a better match between the sound speed in ambient air and the heated but higher atomic weight argon jet. Further investigations of these levitation phenomena may be conducted in the future with an enclosed AAL device which would allow the ambient as well as the levitation jet gas to be controlled.

The results show that high-energy efficiency can be achieved in rapid containerless melt processing of materials. Aluminum oxide specimens of ~ 64 mg mass were heated, melted (at 2327 K), solidified and cooled within 6 s using a CO₂ laser power of ~ 270 W. This is equivalent to a mass rate of 38 g/h and a laser energy consumption rate of 7 kW h/kg (3.2 kW h/pound) of processed material. When it is considered that heating and melting occurred during about half the six-second process period, it is evident that large improvements in the energy efficiency would not be possible. The present results already approach the limiting energy requirement of 1.0 kW h/kg, which equals the enthalpy difference³⁶ between α -aluminum oxide at 298 K and liquid aluminum oxide at the melting point.

V. FUTURE WORK

There are several improvements in the device that may be made in the future. The acoustic driver power supplies and controls can be modified to reduce noise, increase the maximum output power, and provide more precise control

of acoustic phase differences between the pairs of transducers. These changes would achieve improved control of the rotation, shape, and stirring of levitated specimens. An enclosed levitator would also be useful so that the ambient and levitation gas may be made equal for work with gases other than air. The enclosure would allow inert or reducing gas environments to be used and facilitate operation in helium for experiments with increased density materials.

The maximum specimen density that could be levitated in argon was $\sim 9 \text{ g/cm}^3$ and this limit was evidently due to the development of turbulent jet flow at higher gas flow rates. The limit on density may be increased in helium, because the mass flow rate per unit jet momentum flow rate decreases, by a factor of $10^{0.5}$, in the case that helium is substituted for argon. Since the viscosity decreases by a smaller factor,³⁷ i.e., $\mu_{\text{He}}/\mu_{\text{Ar}} \approx 0.8$, the jet Reynolds number at the flow rate required to support the specimen would be about 2.5 times smaller in helium than in argon. Thus it should be possible to levitate denser materials in helium before the onset of turbulent jet flow.

The aerodynamic levitation of solid tungsten in a low-pressure helium jet has actually been demonstrated,³⁸ under conditions for which levitation in an argon gas jet was not possible. However, the present work found that the value of $Re_d h/d$ was ~ 2.5 times smaller in helium than in argon at the point where the height dependence of jet temperature increased. Further experiments will be required with an enclosed levitator, to establish the levitation capabilities for operation with helium gas.

ACKNOWLEDGMENTS

This work was supported by a Small Business Innovative Research Contract from the National Science Foundation and by the Microgravity Sciences and Applications Division of the National Aeronautics and Space Administration.

¹J. K. R. Weber, S. Krishnan, and P. C. Nordine, *J. Metals* **43**, 8 (1991).
²E. H. Trinh, ed., *Proceedings of the 1st Workshop on Containerless Experimentation in Microgravity*, Jan. 17–19, 1990, Jet Propulsion Lab. Pasadena, CA.
³O. Mück, German Patent No. 42204, Oct. 30, 1923.
⁴A. J. Rostron, *Science Journal*, 69–73 (July, 1967).
⁵S. Krishnan, J. K. R. Weber, P. C. Nordine, R. A. Schiffman, R. H. Hauge, and J. L. Margrave, *High Temp. Sci.* **30**, 137 (1991).
⁶C. D. Anderson, W. H. Hofmeister, and R. J. Bayuzick, *Metall. Trans. A* **26**, 2699 (1992).
⁷H. J. Fecht, J. H. Perepezko, M. C. Lee, and W. L. Johnson, *J. Appl. Phys.* **68**, 4494 (1990).
⁸G. Wouch, R. T. Frost, and A. E. Lord, *J. Cryst. Growth.* **37**, 181 (1977).
⁹B. J. Keene, National Physical Laboratory Report DMM(A) 39, Nov. 1991.
¹⁰M. G. Froberg and G. Betz, *Arch. Eisenhüttenw.* **6**, 235 (1980).

¹¹J. A. Treverton and J. L. Margrave, *J. Chem. Thermodyn.* **3**, 473 (1971).
¹²D. W. Bonnell, Ph.D thesis, Rice University, Houston, TX, 1972.
¹³R. Whymark, C. A. Rey, J. Yearnd, and R. Broz, *Proceedings of the 17th Aerospace Sciences Meeting*, New Orleans, LA, 15–17 Jan., 1979.
¹⁴T. G. Wang, M. M. Saffren, and D. D. Elleman, *AIAA Paper No.* 74–155 (1974).
¹⁵P. F. Clancy, E. G. Lierke, R. Grossbach, and W. M. Heide, *Acta Astronaut.* **7**, 877 (1980).
¹⁶E. H. Trinh, J. Robey, N. Jacobi, and T. Wang, *J. Acoust. Soc. Am.* **79**, 3 (1986).
¹⁷C. A. Rey, D. R. Merkley, G. R. Hammarlund, and T. J. Danley, *Metall. Trans.* **19A**, 2619 (1988).
¹⁸C. A. Rey, R. Whymark, T. J. Danley, and D. R. Merkley, in *Materials Processing in the Reduced Gravity Environment of Space*, edited by G. E. Rindone, *Mater. Res. Soc. Symp. Proc. Vol. 9* (Materials Research Society, Pittsburgh, 1982), pp. 137–146.
¹⁹W. K. Rhim, S. K. Chung, and D. D. Elleman, in *Proceedings of the VIIIth European Symposium on Materials and Fluid Sciences in Microgravity*, Oxford, UK, 10–15 Sept. 1989, pp. 629–37.
²⁰S. Arnold, in *Optical Effects Associated with Small Particles*, edited by P. W. Barber and R. K. Chang, *Advanced Series in Appl. Phys.* **1** (World Scientific, Singapore, 1988).
²¹P. Bolsaitis, R. E. Spjut, and J. F. Elliot, *High Temp.–High Pressures* **21**, 601 (1989).
²²E. R. Monazam, D. J. Maloney, and L. O. Lawson, *Rev. Sci. Instrum.* **60**, 3460 (1989).
²³W. K. Rhim, S. K. Chung, D. Barber, K. F. Man, G. Gutt, A. Rulison, and R. E. Spjut, *Rev. Sci. Instrum.* (to be published).
²⁴D. A. Winborne, P. C. Nordine, D. E. Rosner, and N. F. Marley, *Metall. Trans.* **7B**, 711 (1976).
²⁵P. C. Nordine and R. M. Atkins, *Rev. Sci. Instrum.* **53**, 1456 (1982).
²⁶P. C. Nordine, J. K. R. Weber, S. Krishnan, and R. A. Schiffman, *High-Temp. Sci.* **30**, 163 (1991).
²⁷S. Krishnan, P. C. Nordine, J. K. R. Weber, and R. A. Schiffman, *High-Temp. Sci.* **31**, 45 (1991).
²⁸J. P. Coutures, J. C. Rifflet, D. Billard, and P. Coutures, *Proceedings of the 6th European Symposium on Materials Science under Microgravity Conditions*, Noordwijk, The Netherlands, ESA SP-256, pp. 427–430 (1986).
²⁹J. Granier, M. Daniel, C. Parayre, J. Bancillon, and J. P. Bugcat, *Proceedings of the VIII European Symposium on Materials and Fluid Sciences in Microgravity*, European Space Agency, Paris, SP-333, Vol. 1, pp. 349–356 (1992).
³⁰C. S. Ray and D. E. Day, *National SAMPE Tech. Conf. Ser.* **15**, 135 (1983).
³¹J. K. R. Weber, C. D. Anderson, D. R. Merkley, and P. C. Nordine, *J. Am. Ceram. Soc.* (in press).
³²J. K. R. Weber, D. R. Merkley, C. D. Anderson, P. C. Nordine, C. S. Ray, and D. E. Day, *J. Am. Ceram. Soc.* **76**, 2139 (1993).
³³J. K. R. Weber, W. P. Zima, P. C. Nordine, K. C. Goretta, and R. B. Poepfel, in *Containerless Processing Tech. and Appl.*, edited by W. H. Hofmeister and R. A. Schiffman (TMS, Warrendale, PA, 1993), pp. 123–128.
³⁴J. R. Olive, W. H. Hofmeister, R. J. Bayuzick, G. Carro, J. P. McHugh, R. H. Hopkins, M. Vlasse, J. K. R. Weber, P. C. Nordine, and M. McElfresh, *J. Mater. Res.* **9**, 1 (1994).
³⁵C. S. Ray and D. E. Day (private communication).
³⁶M. W. Chase, Jr., C. A. Davies, J. R. Downery, Jr., D. J. Frurip, R. A. McDonald, and A. N. Syverud, *JANAF Thermochemical Tables Third Edition*, *J. Phys. Chem. Ref. Data* **14** (Supplement 1) 1985.
³⁷R. A. Svehla, *NASA Technical Report R-132*, 1962.
³⁸P. C. Nordine, J. K. R. Weber, and S. Krishnan (unpublished research).